nanomaterials

MDPI

Article

First-Principle Insight into Ga-Doped MoS_2 for Sensing SO_2, SOF_2 and SO_2F_2

Wenjun Hou [1], Hongwan Mi [1], Ruochen Peng [1], Shudi Peng [2], Wen Zeng [3,*] and Qu Zhou [1,*]

1 College of Engineering and Technology, Southwest University, Chongqing 400715, China; hwj2401@163.com (W.H.); hongwanmi@163.com (H.M.); ruochenpeng@163.com (R.P.)
2 Chongqing Electric Power Research Institute, State Grid Chongqing Electric Power Company, Chongqing 401123, China; pengshudi@163.com
3 College of Materials Science and Engineering, Chongqing University, Chongqing 400044, China
* Correspondence: wenzeng@cqu.edu.cn (W.Z.); zhouqu@swu.edu.cn (Q.Z.); Tel.: +86-136-5837-6869 (W.Z.); +86-130-683-05845 (Q.Z.)

Abstract: First-principle calculations were carried out to simulate the three decomposition gases (SO_2, SOF_2, and SO_2F_2) of sulfur hexafluoride (SF_6) on Ga-doped MoS_2 (Ga-MoS_2) monolayer. Based on density functional theory (DFT), pure MoS_2 and multiple gas molecules (SF_6, SO_2, SOF_2, and SO_2F_2) were built and optimized to the most stable structure. Four types of Ga-doped positions were considered and it was found that Ga dopant preferred to be adsorbed by the top of Mo atom (T_{Mo}). For the best adsorption effect, two ways of SO_2, SOF_2, and SO_2F_2 to approach the doping model were compared and the most favorable mode was selected. The adsorption parameters of Ga-MoS_2 and intrinsic MoS_2 were calculated to analyze adsorption properties of Ga-MoS_2 towards three gases. These analyses suggested that Ga-MoS_2 could be a good gas-sensing material for SO_2 and SO_2F_2, while it was not suitable for SOF_2 sensing due to its weak adsorption. This work provides a theoretical basis for the development of Ga-MoS_2 materials with the hope that it can be used as a good gas-sensing material for electrical equipment.

Keywords: sulfur hexafluoride; Ga-MoS_2; density functional theory; adsorption properties

Citation: Hou, W.; Mi, H.; Peng, R.; Peng, S.; Zeng, W.; Zhou, Q. First-Principle Insight into Ga-Doped MoS_2 for Sensing SO_2, SOF_2 and SO_2F_2. *Nanomaterials* **2021**, *11*, 314. https://doi.org/10.3390/nano11020314

Academic Editor: Mads Brandbyge
Received: 24 December 2020
Accepted: 15 January 2021
Published: 26 January 2021

1. Introduction

SF_6 is known as a colorless, odorless, non-toxic, and incombustible inert gas [1]. It has an octahedral molecular structure and high chemical stability with short bond length and high bond energy [2]. SF_6 is used for the insulation of Gas-Insulated-Switchgear (GIS) installations and arc extinguishing dielectric due to its extraordinary arc extinguishing property, insulation performance, and adequate chemical steadiness [3]. During the long running times, GIS installations may get some insulation defects such as metal particle defects, metal protrusion defects, air gap defects, etc. [4]. Insulating defects will initiate partial discharge and lead to the disintegration components of SF_6, such as SO_2, SOF_2, and SO_2F_2, etc. [5]. On the one hand, some decomposition products are corrosive, which may cause certain damages to the equipment [6,7]. On the other hand, the stability and insulation of the decomposition gases are far inferior than that of SF_6 [8]. In order to ensure the stable and safe operation of GIS equipment, the specific types and degree of equipment defects could be evaluated by measuring the types and concentrations of SF_6 disintegration components [9]. At present, one of the main methods to detect SF_6 disintegration products is the gas sensor detection method [10]. MoS_2 monolayer is a new member of two-dimensional materials like graphene, which has unique physical, chemical, and electrical characters [11]. According to previous papers, MoS_2 monolayers have a bandgap of 2.06 eV, suitable carrier fluidity, and high thermal stability [12,13]. In general, its unique structure makes it exhibit good gas sensitivity and adsorption characteristics [14]. Furthermore, published literature already proved that some metal or non-metal doping

on MoS_2 monolayers could further enhance their sensitivity to gas molecules [15,16]. The reason was the fit doped atoms regulate the electrons on the surface of MoS_2 monolayers and improve the electron density of the doping points to realize the orbital interaction between the doped atoms and some atoms of the gas molecules [17]. Wang J.X. et al. developed a hydrothermal synthesis of Au-MoS_2 microspheres, whose conductivities were better than that of the intrinsic MoS_2 material [18]. Abbas H.G. et al. modified MoS_2 with non-metallic atoms N and P, and tested the adsorption of O_2 and NO. They found that the adsorption effects of modified N-MoS_2 and P-MoS_2 were stronger than that of intrinsic MoS_2 [19]. Ga is a common semiconductor dopant, which is used as the dopant of nitrogen, arsenic, phosphorus, and other elements. However, as far as we know, the Ga-MoS_2 monolayer has not been reported for its application in SF_6 decomposition products detection.

In this paper, Ga-MoS_2 was selected as sensitive material for adsorption of three typical SF_6 disintegration components (SO_2, SOF_2, and SO_2F_2). We performed density functional theory (DFT) method and simulated the adsorption of three gas molecules onto the intrinsic MoS_2 and Ga-MoS_2, aiming to shed light on its adsorption ability [20,21]. The optimal configuration of each structure, adsorption energy, charge conversion, density of states (DOS), and band structure were calculated through the DFT method [22]. Furthermore, the simulation results were compared, and the conclusions of material adsorption performance were obtained.

2. Computational Details

Our calculations were designed to qualitatively analyze the effects of Ga doping on sensing properties of MoS_2 at the atomic level. The calculation method was basically consistent with the previous research, so that the results were comparable. The adsorption between MoS_2-based materials and gas molecules were studied with the DFT method, which is one of the most effective ways to predict the performance of materials by calculating their electronic structures [23]. The molecular spin-polarized algorithms were achieved using $DMol^3$ package of Material Studio (MS). The generalized gradient approximation (GGA), which is the Perdew–Burke–Ernzerhof (PBE) functional, was chosen to figure out the doping and hybridization between electrons [24,25]. Within the function of MS software, the double numerical plus polarization (DNP) was utilized as the atomic orbital base install. Meanwhile, the DFT semi-core pseudopotential (DSSP) method was selected to deal with the influence of core electron relativity [26–28].

The Brillouin zone of MoS_2 monolayer systems was sampled with k-point of $5 \times 5 \times 1$, and Self-Consistent Field (SCF) convergence criterion was set to 1×10^{-6} Ha [29]. The convergence criteria of geometry optimizations were set to 5×10^{-3} A for displacement, 2×10^{-3} Ha/Å for force, and 10^{-5} Ha for energy [30]. A $4 \times 4 \times 1$ MoS_2 monolayer supercell was built, including 16 Mo and 32 S atoms with a vacuum zone of 15 Å [31].

In this paper, the difficulty of doping could be judged by analyzing the energy of formation, adsorption energy, and charge transfer capacity.

We obtained the energy of formation (E_{form}) through the calculation:

$$E_{form} = E_{Ga-MoS_2} - E_{MoS_2} - E_{Ga} \quad (1)$$

E_{Ga-MoS_2} is the energy of the system after Ga doping. E_{MoS_2} and E_{Ga} denote the energy of pure MoS_2 and Ga atom, respectively [32,33].

The adsorption energy (E_{ad}) of each gas molecules on Ga-MoS_2 monolayer were calculated by the following equation:

$$E_{ad} = E_{Ga-MoS_2/gas} - E_{Ga-MoS_2} - E_{gas} \quad (2)$$

$E_{Ga-MoS_2/gas}$ is the total energy of gas-adsorbed Ga-MoS_2 monolayers and E_{gas} represents the energy of gas molecules before adsorption [34,35].

Mulliken charge characterized the number of electrons carried by gas molecules adsorbed. It was utilized to calculate the charge transfer between Ga-MoS_2 and gas molecules. The definition of charge transfer (Q_t) used in this paper is:

$$Q_t = Q_{adsorbed(gas)} - Q_{isolated(gas)} \quad (3)$$

$Q_{adsorbed(gas)}$ and $Q_{isolated(gas)}$ mean the number of charges carried by gas molecules before and after adsorption. Normally, the figure of $Q_{adsorbed(gas)}$ is zero. If electrons are shifted from gas molecules to Ga-MoS_2 monolayers, Q_t is positive [36–38].

3. Results and Discussion

3.1. Geometric Structure of Gas Molecules, MoS_2, and Ga-MoS_2 Monolayer

First, the geometric structures of SF_6, SO_2, SOF_2, and SO_2F_2 were optimized to their steadiest configuration before studying their adsorption. Figure 1 displays the four structures and the information of bond lengths and angles are shown in Table 1.

Table 1. Structural parameters of gas molecules.

Gas Molecule	Bond Length (Å)		Bond Angle (°)	
SF_6	S-F	1.64	F-S-F	90.3
SO_2	S-O	1.48	O-S-O	119.94
SOF_2	S-F	1.67	O-S-F	107.14
	S-O	1.46	F-S-F	93.039
$SO2F_2$	S-F	1.61	O-S-O	126.73
	S-O	1.44	O-S-F	107.74
	-		F-S-F	94.44

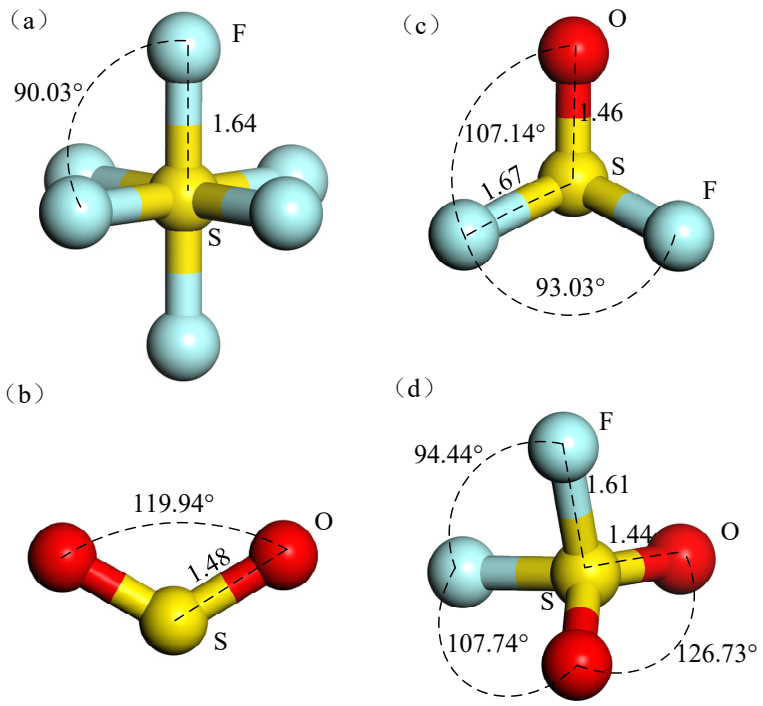

Figure 1. Structures of (**a**) SF_6, (**b**) SO_2, (**c**) SOF_2, (**d**) SO_2F_2.

A SF_6 molecule has a regular octahedral structure with six F atoms arranged symmetrically around an S atom. It is difficult to accumulate enough energy for collision ionization because of the large molecular diameter of SF_6. When electrons attach and collide with SF_6 molecules, energy loss will increase and further weaken its ionization ability. Form Figure 1b, the SO_2 molecule had structure presenting a highly symmetrical "V" shape.

SOF_2 molecule presented a tetrahedral structure, as shown in Figure 1c. SO_2F_2 molecule had a similar structure to SOF_2. Figure 1d indicates that SO_2F_2 was symmetrical about the plane where the mid-perpendicular line of two F atoms or two O atoms were connected. The bond length and bond angle of the optimized structure of these gases were consistent with the previous reference [39]. The optimized pure MoS2 monolayer is shown in Figure 2a. The bandgap of the optimized structure is displayed in Figure 3a. The energy gap was 2.06 eV, which was less than the experimental value (3.2 eV) and consistent with the simulation value (2.06 eV) [40]. It indicates that the energy required for the electrons to jump between the valence band and conduction band was large and the electrons were difficult to be excited.

Four types of Ga-doped positions on pure MoS_2 monolayers were considered, which were T_S (at the top of the S atom) in Figure 2b, $B_{S\text{-}S}$ (the bridge site between two S atoms) in Figure 2c, T_{Mo} (at the top of the Mo atom) in Figure 2d, and T_H (above the hexagonal ring center of MoS_2) in Figure 2e, respectively [41].

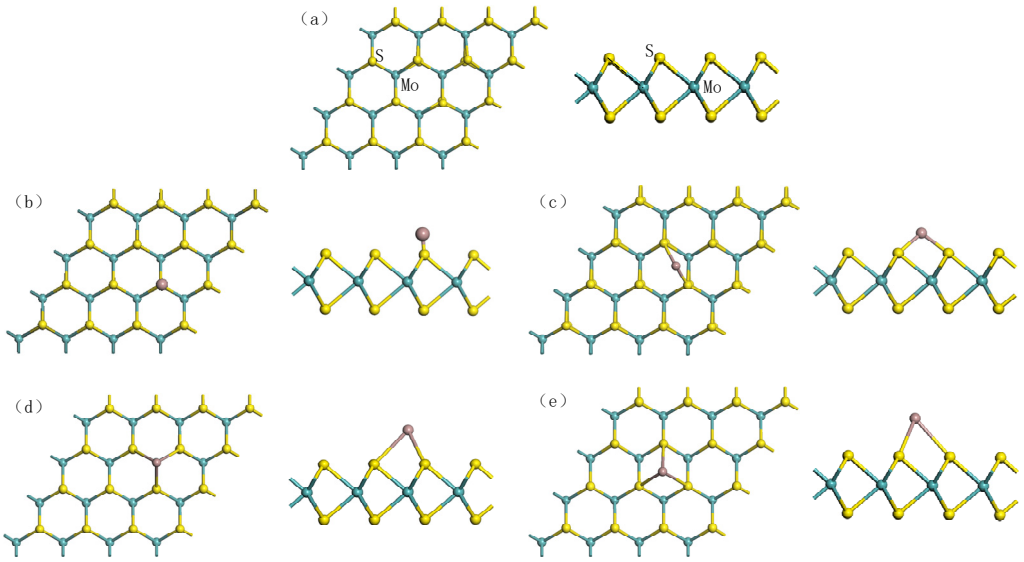

Figure 2. Structure of (**a**) pure MoS_2, (**b**) T_S site, (**c**) $B_{S\text{-}S}$ site, (**d**) T_{Mo} site, (**e**) T_H site.

As shown in Table 2, we calculated E_{form} for the four Ga doping models. It was evident that the most favorable doping position had the lowest formation energy, which means that the reaction occurred most easily [42,43]. The T_{Mo} site had the smallest formation energy of −1.75 eV. Therefore, for the optimization model obtained by the four ways Ga can be doped on MoS_2, the optimization model of T_{Mo} position was the best. From the bond-forming parameters, Ga atoms preferred to approach MoS_2 monolayers from the top of Mo atoms. Three of Ga-S bonds were formed between Ga and MoS_2 monolayers, all of which were closed to 2.70 Å in length, indicating the strong interaction between Ga and S atoms. The results show that the surface structure of MoS_2 did not change much with the doping of Ga. The bond angles of Mo-S-Mo and S-Mo-S were 81.225° and 82.445°, respectively, which had little change from 81.962° before doping. Simultaneously, the distance between the Ga atom and Mo atom was a bit long (3.55 Å), showing the inferior attractive force between them. In conclusion, Figure 2d displays the most stable structure, which is the optimal model used for subsequent adsorption calculations.

Table 2. Formation energy of the four Ga-doping models.

Doping Sites	T_S	$B_{S\text{-}S}$	T_{Mo}	T_H
E_{form}(eV)	−1.70	−1.74	−1.75	−1.60

Figure 3 displays the bandgap structures comparison before and after the Ga doping of MoS_2. Besides, to compare more intuitively the similarities or differences of electronic structures before and after Ga doping, the DOS contrast was carried out as displayed in Figure 4. In Figure 3, the bandgap between the valence band and conduction band decreased to 1.90 eV. The separation distance corresponds to the width between the two peaks near the Fermi level of DOS. Figure 4 shows that the total density of states (TDOS) shifted to the lower energy direction compared with that before Ga doping. From the Fermi level, it can be seen that the distance between the valence band and the conduction band shortened. It shows that the conductivity of Ga-MoS_2 ameliorated due to the doping of Ga.

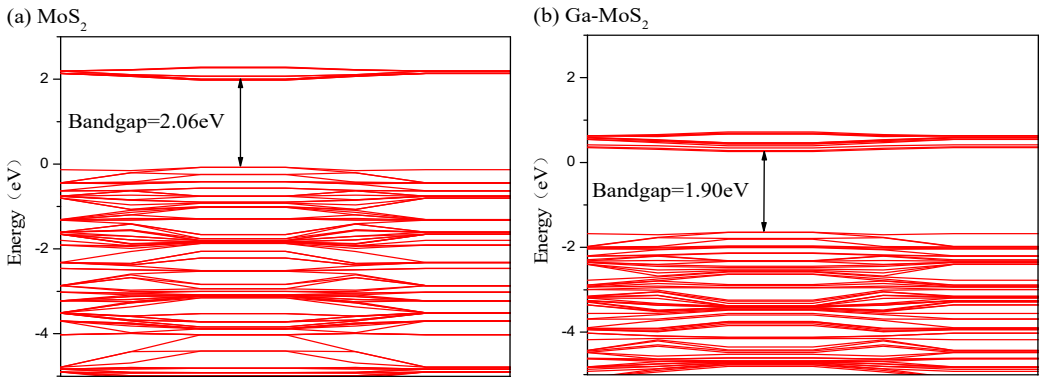

Figure 3. The energy band of (**a**) MoS_2 (**b**) Ga-MoS_2 system.

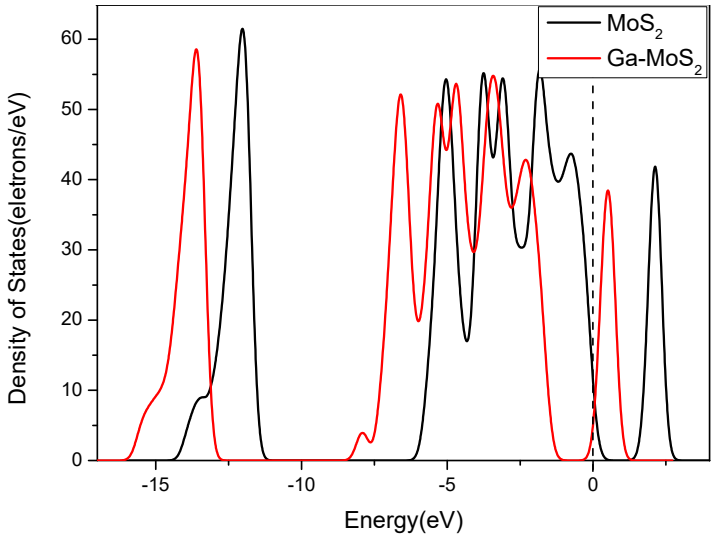

Figure 4. The density of states (DOS) curves comparison before and after doping. The dotted lines are Fermi level.

3.2. Adsorption Analysis of Ga-MoS_2 Monolayer to Gas Molecules

3.2.1. Adsorption Analysis of MoS_2 Monolayer to Gas Molecules

As Figure 5 shows, the optimized pure MoS_2 model was used to adsorb the three target gases. The adsorption parameters of three gas adsorption systems listed in Table 3, including adsorption distance (D), E_{ad}, and Q_t [44]. The adsorption distance between gas molecules and MoS_2 was large in the adsorption model, which indicates that intrinsic MoS_2 had weak adsorption capacity for the three gases. It also can see the adsorption of SO_2, SOF_2 by MoS_2 tended to be close to S atom in SO_2 and SOF_2 molecules, while SO_2F_2 molecule was close to O atom. The S-F bond was slightly elongated in SO_2F_2 molecule. As seen in Table 3, the adsorption energies of the three target gases were all positive, indicating that the reaction was endothermic and could not be spontaneous. It proves

that the intrinsic MoS_2 had low adsorption effect on the target gases. The bond angles of SO_2, SOF_2, and SO_2F_2 were reduced to a certain extent after being adsorbed. The charge transfer values of SO_2, SOF_2, and SO_2F_2 were negative, and mean that electrons shifted from MoS_2 surface to gas molecules during the adsorption process. However, the electrons were not active during the adsorption process due to the micro charge transfer in the three adsorption systems. In summary, the intrinsic MoS_2 had a weak adsorption capacity for the target gases. The improved adsorption performance of MoS_2 required doping of metal or non-metal atoms.

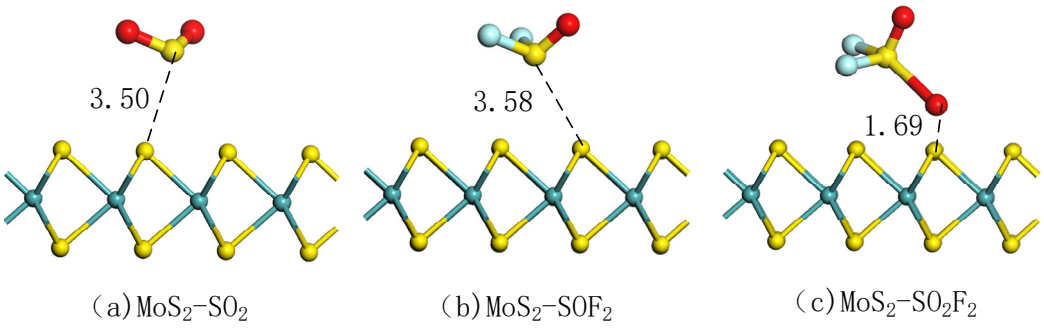

Figure 5. Adsorption structures of MoS_2 for (**a**) SO_2 (**b**) SOF_2 (**c**) SO_2F_2.

The band structures of the adsorption systems corresponding to the three gases were analyzed, as shown in Figure 6. The bandgap of the intrinsic MoS_2 was 2.06 eV according to the previous calculation. It can be seen from Figure 6a, the bandgap decreased to 0.57 eV after adsorption of SO_2 molecule, indicating that electrons more easily transited from the valence band to the conduction band, and the conductivity of system significantly improved after adsorption [45]. Figure 6b displays that the bandgap of the SOF_2 molecule adsorption system reduced by 0.67 eV, illustrating that the conductivity of the system was raised. Figure 6c demonstrates that the bandgap of the SO_2F_2 molecule adsorption system diminished by 0.33 eV, the bandgap changed less than the other two gases, and the system's conductivity did not change evidently. Overall, the bandgap of MoS_2 decreased most obviously after SO_2 molecule adsorption.

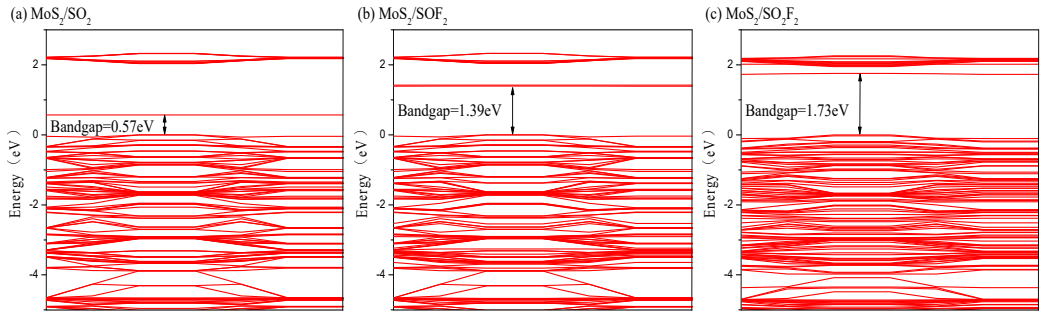

Figure 6. The energy band of (**a**) MoS_2/SO_2 (**b**) MoS_2/SOF_2 (**c**) MoS_2/SO_2F_2 adsorption system.

Table 3. Parameters of adsorption of the target gases on MoS_2 surface.

Gas Molecules	D (Å)	E_{ad}(eV)	Q_t(e)	Structure	
SO_2	3.50	22.34	−0.04	∠ O-S-O	112.64
SOF_2	3.58	22.41	−0.04	∠ O-S-F ∠ F-S-F	104.10 95.73
SO_2F_2	1.69	25.03	−0.68	∠ O-S-O ∠ O-S-F ∠ F-S-F	100.17 95.38 94.08

3.2.2. Selection of Adsorption Modes for Gas Molecules in Ga-MoS_2 Monolayer

For the best adsorption effect, two ways for SO_2, SOF_2, and SO_2F_2 to approach the doping model were compared [46], as shown in Figure 7. The parameters of gas adsorption on Ga-MoS_2 in different approaches are listed in Table 4.

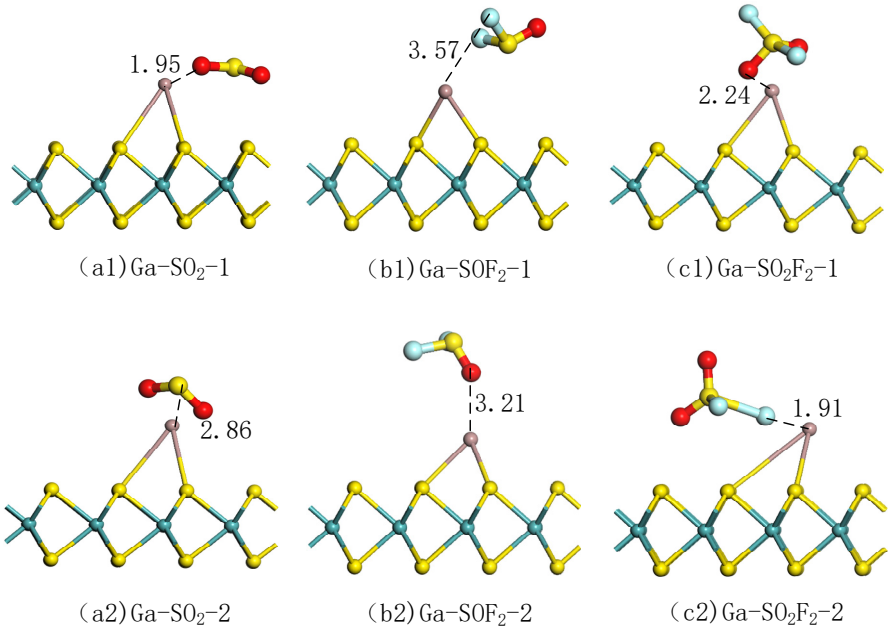

Figure 7. Structure of (**a1**,**a2**) SO_2 adsorption mode, (**b1**,**b2**) SOF_2 adsorption mode, (**c1**,**c2**) SO_2F_2 adsorption mode.

Table 4. Parameters of gas adsorption on Ga-MoS2 in different approaches.

Parameters	SO2		SOF2		SO2F2	
Approach	Mode 1	Mode 2	Mode 1	Mode 2	Mode 1	Mode 2
D (Å)	Ga-O:1.95	Ga-S:2.86	Ga-F:3.57	Ga-O:3.21	Ga-O:2.24	Ga-F:1.91
E_{ad}(eV)	−0.61	−0.67	0.36	0.27	−0.15	−0.63
Q_t(e)	−0.40	−0.42	−0.01	0.01	−0.59	−0.60

As Figure 7(a1,a2) shows, two types of SO_2 adsorption models were built: O atom or S atom near the Ga atom. It can be seen that in the adsorption system obtained after optimization by mode 2, approach mode had changed, while the approach mode 1 had not changed, basically. In the two modes, SO_2 lost electrons and the Ga-MoS_2 doping model gained electrons. After calculation, the numerical value of the E_{ad} of the adsorption model constructed in mode 2 was more significant than that constructed in mode 1. At the same time, the absolute value of Q_t of the former was larger than that of the latter, and both are negative. It shows that the adsorption process approached in mode 2 was more intense. It also displays that Ga-MoS_2 was more inclined to mode 2 for the adsorption of SO_2. Therefore, the adsorption structure obtained by mode 2 was selected as the best structure to facilitate follow-up analysis.

It could be obtained from the above analysis that the adsorption process in the way that S atoms approach the doping model was difficult to occur. This paper adopts two gas approach modes for the adsorption of SOF_2. The one was mode 1 that approaches F atoms' doped structure. The other was mode 2, which was approaching the doped structure with O atoms as Figure 7(b1,b2) shows. After optimization calculations, the two adsorption modes were basically unchanged, but the adsorption distance was relatively long. The doping model had a weaker adsorption effect on SOF_2 for both the approach methods. Both of their adsorption energies were positive, and the amount of charge transfer was very

small and close to zero. It proved the adsorption effect of Ga-MoS_2 on SOF_2 was not ideal. However, considering the completeness of the analysis and comparison, mode 2, which has lower adsorption energy, was selected in this paper for the subsequent calculation.

Similarly, for the adsorption of SO_2F_2, two adsorption methods were selected in this paper. One was to use O atoms to approach the doped structure in Figure 7(c1) and the other was to use F atoms to approach the doped model in Figure 7(c2). It can be seen that the two adsorption methods had not changed to a large extent after optimization calculation. In addition, both SO_2F_2 and Ga-MoS_2 had a certain degree of deformation in mode 2. Among them, an S-F bond of the SO_2F_2 was elongated, and the bond between Ga and MoS_2 was also elongated, which shows that the adsorption process was relatively strong. In comparison, mode 2 had larger adsorption energy and charge transfer amount than mode 1, which also proved that the adsorption process was stronger. In summary, the adsorption model obtained by mode 2 was better for Ga-MoS_2 adsorption of SO_2F_2, so it was selected as the subsequent energy band and DOS analysis.

In order to show the varieties of structural parameters before and after adsorption, D, E_{ad}, Q_t and some structural parameters of mode 2 are listed in Table 5. Among all the adsorption models of Ga-MoS_2, the E_{ad} of SO_2 and SO_2F_2 were both negative, indicating that Ga-MoS_2 could adsorb the above two gases more stably. At the same time, the E_{ad} of SOF_2 was positive, which suggests that Ga-MoS_2 had some difficulty in adsorption of SOF_2.

Table 5. The parameters for the target gases on the Ga-MoS_2 surface.

Gas Molecule	D (Å)	E_{ad}(eV)	Q_t(e)	Gas Structure		$d_{Ga\text{-}S}$ (Å)	∠ S-Ga-S (°)
SO_2	2.30	−0.67	−0.42	∠ O-S-O	105.53	3.32	52.80
SOF_2	3.21	0.27	0.01	∠ O-S-F ∠ F-S-F	106.76 93.543	2.66	71.19
SO_2F_2	1.91	−0.63	−0.60	∠ O-S-O ∠ O-S-F ∠ F-S-F	121.60 105.25 88.32	2.94	48.62

3.2.3. Energy Band and DOS Analysis

For the sake of further discussions about electronic characteristics of the model obtained by adsorption, the energy band structure and DOS of the three adsorption models were analyzed [47,48]. Figure 8 shows the band structure diagram of the adsorption system obtained by pure MoS_2 and Ga-MoS_2 adsorbing SO_2, SOF_2, and SO_2F_2.

It can be seen from the above description that the bandgap of Ga-MoS_2 without adsorbed gas was 1.90 eV. Figure 8a displays the energy band structure diagram of the adsorption system after Ga-MoS_2 adsorbed SO_2. The energy bandgap of the system reduced to 0.60 eV, which shows that the adsorption of SO_2 could make the electrical conductivity of the material promoted to a certain extent. From Figure 8b, it can be seen that after SOF_2 adsorption, the bandgap of the adsorbed system dropped to 1.76 eV. This indicates that electrons could more likely transition from the valence band to the conduction band than the unabsorbed system. As a result, the conductivity of the material had been improved. Figure 8c displays that after the doped structure adsorbs SO_2F_2, the bandgap of the adsorption system becomes 1.93 eV, which is an increase of 0.03 eV compared to the bandgap of the system without gas adsorption. The energy minimum band distance increases slightly. The conductivity of the entire system decreases, but the decrease in the conductivity of the system was very limited due to the small bandgap increase. Thus, the adsorption of SO_2F_2 hardly influences the conductivity of Ga-MoS_2 monolayer.

To sum up, the conductivity of the material could be improved to varying degrees by adsorbing SO_2 and SOF_2. At the same time, adsorption of SO_2F_2 reduced slightly the conductivity of the material.

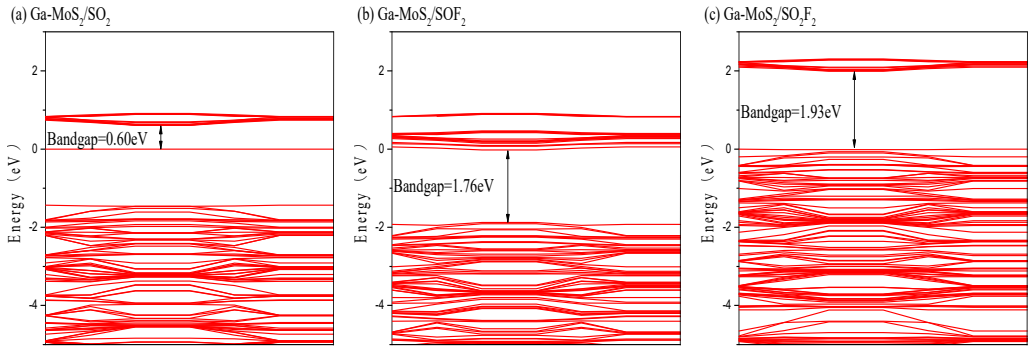

Figure 8. The energy band of (**a**) Ga-MoS_2/SO_2 (**b**) Ga-MoS_2/SOF_2 (**c**) Ga-MoS_2/SO_2F_2adsorption system.

Figures 9–11 show the DOS of Ga-MoS_2 for SO_2, SOF_2, and SO_2F_2 adsorption structures, divided into TDOS and partial density of states (PDOS).

Figure 9a represents the comparison of the TDOS of the system before and after the adsorption of SO_2. As shown, the TDOS of Ga-MoS_2 had eight peaks before adsorption of SO_2. After the adsorption of SO_2, the adsorption system added a new peak near −10 eV, which indicates that the electron orbit of the adsorption system had changed during the adsorption process. At the same time, the TDOS of the system after adsorption was slightly shifted to the right compared with that before the adsorption. After the adsorption of SO_2, the peak value of TDOS near 1 eV had increased, and electrons gathered at the bottom of the conduction band. So, the conductivity of the material had been improved to a certain extent. According to the PDOS of Ga-MoS_2 for SO_2 adsorption displayed in Figure 9b, the DOS of the listed atoms were mainly distributed in the range of −7.5~0 eV. The hybridization primarily occurred between the 4p orbital of Ga and the 2p orbital of O, and the PDOS of −7.5~−5 eV and −2.5~2.5 eV regions with varying degrees of overlap. At the same time, the 3p orbital of S had the most DOS distribution at the Fermi level. It can be inferred that S had the greatest influence on the electrical conductivity of the entire material in this adsorption system.

Figure 10a displays the TDOS changes of the system before and after SOF_2 adsorption. The TDOS of the Ga-MoS_2 system after adsorption had three new peaks. Additionally, the TDOS after adsorption was slightly moved to the left compared to the system before adsorption. The TDOS at the Fermi level had the obvious increase, meaning that the electrical conductivity of the entire system had been improved after being gas adsorbed. The electrons were more likely to jump to the conduction band. The PDOS of the system could be obtained in Figure 10b. The S-3p, F-2p, and Ga-4p orbitals mainly distributed in the range of −12.5~−5 eV. The hybridization of the system was mostly between the 4p orbital of Ga and the 2p orbital of F. At the same time, it can be seen that in this adsorption system, the 3p orbital of S has the most DOS distribution at the Fermi level. It be concluded that, in this system, S had the strongest influence on the electrical conductivity of the material.

From Figure 11a, the TDOS of the entire system had a more obvious shift to the right after SO_2F_2 was adsorbed. Focusing on the Fermi level, it is found that the DOS at the Fermi level does not change much before and after adsorption, which indicates that the conductivity of the entire system changed slightly after adsorption of SO_2F_2. Figure 11b shows the PDOS of the adsorption system. The DOS of each atom was mainly distributed in the range of −7.5~0 eV. The 4s orbital of Ga and the 2p orbital of F overlap obviously, suggesting that the hybridization of the above-mentioned two orbitals was mainly during the adsorption process. At the same time, it can be seen that in this adsorption system, at the Fermi level, the 4s orbital state density distribution of Ga is the largest, which means that in this adsorption system, the electrical conductivity of the material is mainly affected by Ga atom.

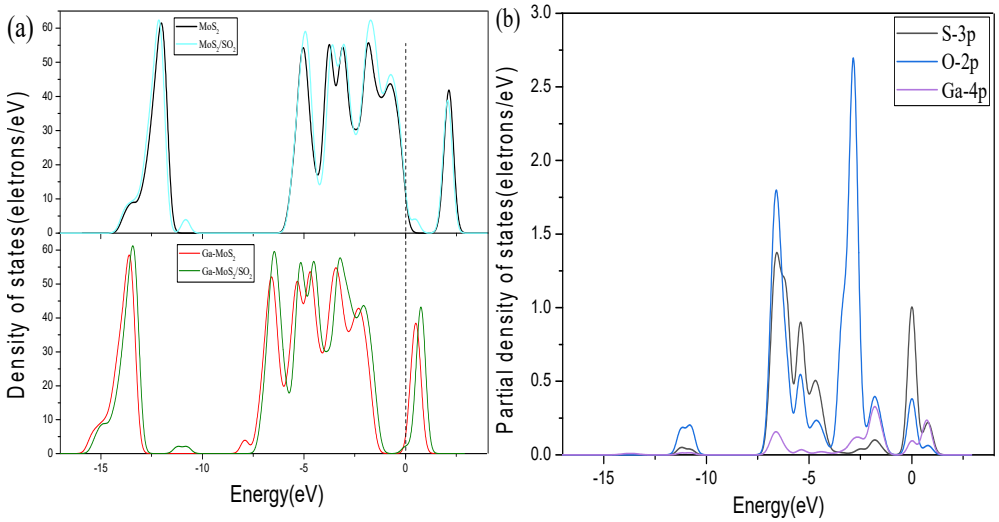

Figure 9. Comparative analysis of (**a**) DOS and (**b**) PDOS for SO_2 system. The dotted lines are Fermi level.

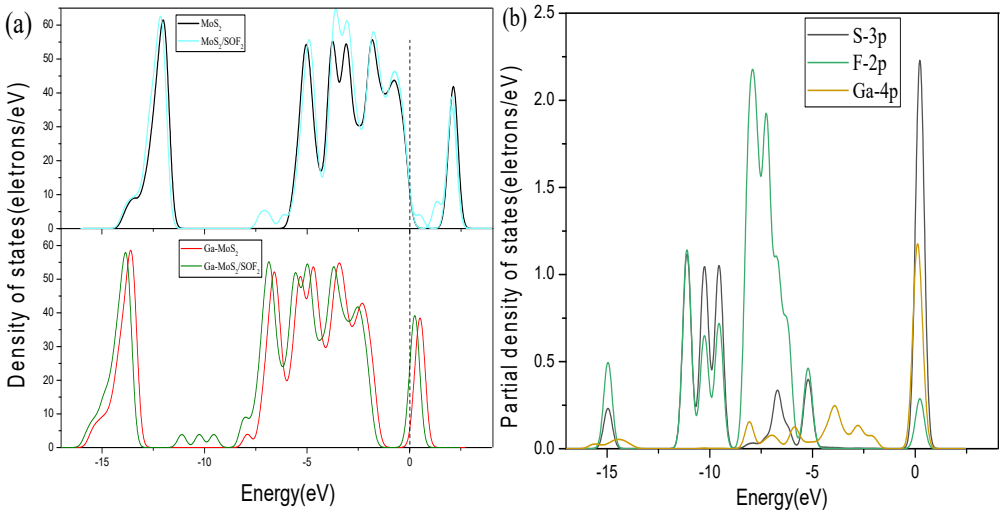

Figure 10. Comparative analysis of (**a**) DOS and (**b**) PDOS for SOF_2 system. The dotted lines are Fermi level.

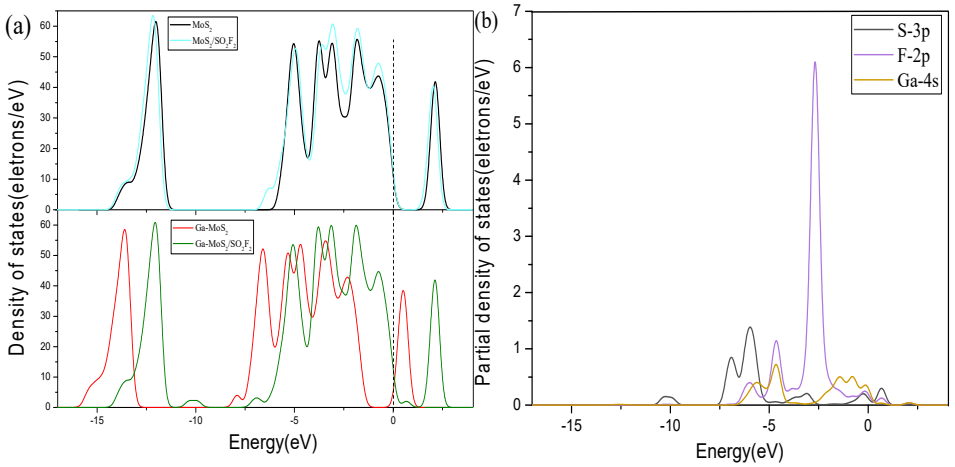

Figure 11. Comparative analysis of (**a**) DOS and (**b**) PDOS for SO_2F_2 system. The dotted lines are Fermi level.

4. Conclusions

In this work, theoretical calculations were carried out to study the adsorption properties of Ga-MoS_2 for SO_2, SOF_2, and SO_2F_2. The positions of Ga doping were considered. The two ways of gas molecules to approach the doping model were compared. The adsorption parameters, energy bands, and DOS were calculated and analyzed. The main conclusions are as follows:

1. Ga dopant was most likely to be adsorbed onto the MoS_2 monolayer through T_{Mo} site.
2. The intrinsic MoS_2 had a weak adsorption capacity for the target gases.
3. SO_2 molecule tends to approach the doped model with S atoms. SOF_2 molecule prefers to approach the doped model with O atoms. SO_2F_2 molecule is likely to approach the doped model with F atoms.
4. The conductivity of the material could be improved to varying degrees by adsorbing SO_2, SOF_2, while adsorption of SO_2F_2 had little effect on the conductivity of the material. The E_{ad} of SO_2 and SO_2F_2 were both negative, indicating that Ga-MoS_2 could adsorb the above two gases more stably. The E_{ad} of SOF_2 is positive, which proves that Ga-MoS_2 had some difficulty in adsorption of SOF_2. The Ga-MoS_2 can be used as an excellent gas-sensing material for SO_2 and SO_2F_2 molecules.

Author Contributions: Conceptualization, W.H. and H.M.; Data curation, W.H.; Investigation, W.H. and H.M.; Methodology, W.H. and Q.Z.; Project administration, W.Z. and Q.Z.; Resources, S.P.; Supervision, Q.Z.; Validation, H.M., R.P. and S.P.; Visualization, R.P.; Writing–original draft, W.H.; Writing—review and editing, W.H., H.M., R.P., W.Z. and Q.Z. All authors have read and agreed to the published version of the manuscript.

Funding: This research was funded by the National Natural Science Foundation of China (Nos. 52077177 and 51507144) and Fundamental Research Funds for the Central Universities (No. XDJK2019 B021).

Informed Consent Statement: Not applicable.

Data Availability Statement: The data is available on the request from corresponding author.

Conflicts of Interest: The authors declare no conflict of interest.

References

1. Zeng, F.P.; Li, H.T.; Zhang, M.X.; Li, C.; Yao, Q.; Tang, J. Establishment of Reax force field of SF6 gas over-thermal decomposition. *J. Phys. D Appl. Phys.* **2020**, *26*, 125540.
2. Zhang, X.X.; Cui, Z.L.; Yi, L.; Li, Y.L.; Xiao, H.Y.; Chan, D.C. Theoretical study of the interaction of SF_6 molecule on Ag (1 1 1) surfaces. *Appl. Surf. Sci.* **2018**, *457*, 745–751. [CrossRef]
3. Liu, H.C.; Zhou, Q.; Zhang, Q.Y.; Hong, C.X.; Xu, L.N.; Jin, L.F.; Chen, W.G. Synthesis, Characterization and Enhanced Sensing Properties of a NiO/ZnO p-n Junctions Sensor for the SF_6 Decomposition Byproducts SO_2, SO_2F_2, and SOF_2. *Sensors* **2017**, *17*, 913. [CrossRef]
4. Wang, J.X.; Zhou, Q.; Zeng, W. Competitive adsorption of SF6 decompositions on Ni-doped ZnO (100) surface: Computational and experimental study. *Appl. Surf. Sci.* **2019**, *479*, 185–197. [CrossRef]
5. Tang, J.; Zeng, F.; Pan, J.; Zhang, X.X.; Yao, Q.; He, J.; Hou, X. Correlation analysis between formation process of SF_6 decomposed components and partial discharge qualities. *IEEE Trans. Dielectr. Electr. Insul.* **2013**, *20*, 864–875. [CrossRef]
6. Dasgupta, U.; Chatterjee, S.; Pal, A.J. Thin-film formation of 2D MoS_2 and its application as a hole-transport layer in planar perovskite solar cells. *Sol. Energ. Mat. Sol. C* **2017**, *172*, 353–360. [CrossRef]
7. Zeng, F.P.; Li, H.T.; Zhang, M.X.; Lei, Z.C.; Li, C.; Tang, J. Isotope Tracing Experimental Study on the Effects of Trace H_2O on the Over-Thermal Decomposition of SF_6. *J. Phys. D Appl. Phys.* **2020**, *53*, 355501. [CrossRef]
8. Abbasi, A.; Sardroodi, J.J. Adsorption of O_3, SO_2 and SO_3 gas molecules on MoS_2 monolayers: A computational investigation. *Appl. Surf. Sci.* **2019**, *469*, 781–791. [CrossRef]
9. Zhang, X.X.; Ren, J.B.; Tang, J.; Sun, C.X. Kernel statistical uncorrelated optimum discriminant vectors algorithm for GIS PD recognition. *IEEE Trans. Dielectr. Electr. Insul.* **2009**, *16*, 206–213. [CrossRef]
10. Chen, D.C.; Tang, J.; Zhang, X.X.; Li, Y.; Liu, H.J. Detecting decompositions of sulfur hexafluoride using MoS_2 monolayer as gas sensor. *IEEE Sens. J.* **2019**, *19*, 39–46. [CrossRef]

11. Zhang, D.Z.; Jiang, C.X.; Wu, J.F. Layer-by-layer assembled In_2O_3 nanocubes/flower-like MoS_2 nanofilm for room temperature formaldehyde sensing. *Sens. Actuators B Chem.* **2018**, *273*, 176–184. [CrossRef]
12. Fan, C.; Liu, G.Z.; Zhang, Y.H.; Wang, M.J. Synthesis and gas-responsive characteristics to methanol and isopropanol of bean-sprout-like MoS_2. *Mater. Lett.* **2017**, *209*, 8–10. [CrossRef]
13. Wu, S.Y.; Zeng, F.P.; Tang, J.; Yao, Q.; Miao, Y. Triangle Fault Diagnosis Method for SF_6 Gas Insulated Equipment. *IEEE Trans. Power Del.* **2019**, *34*, 1470–1477. [CrossRef]
14. Zhang, X.X.; Gui, Y.G.; Dong, X.C. Preparation and application of TiO_2 nanotube array gas sensor for SF_6-insulated equipment detection: A review. *Nanoscale Res. Lett.* **2016**, *11*, 302. [CrossRef]
15. Cho, B.; Yoon, J.; Lim, S.K.; Kim, A.R.; Kim, D.H.; Park, S.G.; Kwon, J.D.; Lee, Y.J.; Lee, K.H.; Lee, B.H. Chemical sensing of 2D graphene/MoS_2 heterostructure device. *ACS Appl. Mater. Inter.* **2015**, *7*, 16775–16780. [CrossRef]
16. Zeng, F.P.; Lei, Z.C.; Yang, X.; Tang, J.; Yao, Q.; Miao, Y.L. Evaluating the DC Partial Discharge Based on SF_6 Decomposition Characteristics. *IEEE Trans. Power Del.* **2019**, *34*, 1383–1392. [CrossRef]
17. Wu, P.; Yin, N.Q.; Li, P.; Cheng, W.J.; Huang, M. The adsorption and diffusion behavior of noble metal adatoms (Pd, Pt, Cu, Ag and Au) on a MoS_2 monolayer: A first-principles study. *Phys. Chem. Chem. Phys.* **2017**, *19*, 20713–20722. [CrossRef]
18. Wang, J.X.; Zhou, Q.; Lu, Z.R.; Wei, Z.J.; Zeng, W. Gas sensing performances and mechanism at atomic level of Au-MoS_2 microspheres. *Appl. Surf. Sci.* **2019**, *490*, 124–136. [CrossRef]
19. Abbas, H.G.; Debela, T.T.; Hussain, S.; Hussain, I. Inorganic molecule (O_2, NO) adsorption on nitrogen- and phosphorus-doped MoS_2 monolayer using first principle calculations. *RSC Adv.* **2018**, *8*, 38656–38666. [CrossRef]
20. Gao, X.; Zhou, Q.; Wang, J.X.; Xu, L.N.; Zeng, W. Adsorption of SO2 molecule on Ni-doped and Pd-doped graphene based on first-principle study. *Appl. Surf. Sci.* **2020**, *517*, 146180. [CrossRef]
21. Li, T.; Gui, Y.; Zhao, W.; Tang, C.; Dong, X. Palladium modified MoS_2 monolayer for adsorption and scavenging of SF_6 decomposition products: A DFT study. *Phys. E* **2020**, *123*, 114178. [CrossRef]
22. Azofra, L.M.; Sun, C.H.; Cavallo, L.; MacFarlane, D.R. Feasibility of N_2 binding and reduction to ammonia on Fe-deposited MoS_2 2D sheets: A DFT study. *Chem. Eur. J.* **2017**, *23*, 8275–8279. [CrossRef] [PubMed]
23. Zhou, Q.; Zeng, W.; Chen, W.G.; Xu, L.N.; Kumar, R.; Umar, A. High sensitive and low-concentration sulfur dioxide (SO2) gas sensor application of heterostructure NiO-ZnO nanodisks. *Sens. Act. B Chem.* **2019**, *298*, 126870. [CrossRef]
24. Wang, J.X.; Zhou, Q.; Wei, Z.J.; Xu, L.N.; Zeng, W. Experimental and theoretical studies of Zn-doped MoO3 hierarchical microflower with excellent sensing performances to carbon monoxide. *Ceram. Inter.* **2020**, *46*, 29222–29232. [CrossRef]
25. Wang, M.; Wang, W.; Ji, M.; Cheng, X. Adsorption of phenol and hydrazine upon pristine and X-decorated (X=Sc, Ti, Cr and Mn) MoS_2 monolayer. *Appl. Surf. Sci.* **2018**, *439*, 350–363. [CrossRef]
26. Chen, D.C.; Zhang, X.X.; Tang, J.; Cui, H.; Li, Y. Noble metal (Pt or Au)-doped monolayer MoS_2 as a promising adsorbent and gas-sensing material to SO_2, SOF_2 and SO_2F_2: A DFT study. *Appl. Phys. A Mater. Sci. Process.* **2018**, *124*, 194. [CrossRef]
27. Gui, X.X.; Zhou, Q.; Peng, S.D.; Xu, L.N.; Zeng, W. Dissolved gas analysis in transformer oil using Sb-doped graphene: A DFT study. *Appl. Surf. Sci.* **2020**, *533*, 147509. [CrossRef]
28. Wang, Y.; Li, D.; Lai, X.; Liu, B.; Chen, Y.; Wang, F.; Wang, R.; Zhang, L. Direct observation of the hysteretic Fermi level modulation in monolayer MoS_2 field effect transistors. *Curr. Appl. Physics.* **2020**, *20*, 293–303. [CrossRef]
29. Gui, Y.G.; Wang, Y.; Duan, S.K.; Tang, C.; Zhou, Q.; Xu, L.N.; Zhang, X.X. Ab Initio Study of SOF_2 and SO_2F_2 Adsorption on Co-MoS_2. *ACS Omega* **2019**, *4*, 2517–2522. [CrossRef]
30. Zhou, Q.; Xu, L.N.; Umar, A.; Chen, W.G.; Kumar, R. Pt nanoparticles decorated SnO_2 nanoneedles for efficient CO gas sensing applications. *Sens. Act. B Chem.* **2018**, *256*, 656–664. [CrossRef]
31. Jiang, C.X.; Zhang, D.Z.; Yin, N.L.; Yao, Y.; Shaymurat, T.; Zhou, X.Y. Acetylene Gas-Sensing Properties of Layer-by-Layer Self-Assembled Ag-Decorated Tin Dioxide/Graphene Nanocomposite Film. *Nanomaterials* **2017**, *7*, 278. [CrossRef] [PubMed]
32. Gao, X.; Zhou, Q.; Wang, J.X.; Xu, L.N.; Zeng, W. Enhanced ethanol sensing and mechanism of Cr-doped ZnO nanorods: Experimental and computational study. *Ceram. Int.* **2017**, *43*, 14873–14879.
33. Zhou, Q.; Chen, W.G.; Xu, L.N.; Kumar, R.; Gui, Y.G.; Zhao, Z.Y.; Tang, C.; Zhu, S.P. Highly sensitive carbon monoxide (CO) gas sensors based on Ni and Zn doped SnO2 nanomaterials. *Ceram. Int.* **2018**, *44*, 4392–4399. [CrossRef]
34. Cui, H.; Zhang, X.X.; Zhang, G.Z.; Tang, J. Pd-doped MoS_2 monolayer: A promising candidate for DGA in transformer oil based on DFT method. *Appl. Surf. Sci.* **2019**, *470*, 1035–1042. [CrossRef]
35. Gui, X.X.; Zhou, Q.; Peng, S.D.; Xu, L.N.; Zeng, W. Adsorption behavior of Rh-doped MoS_2 monolayer towards SO_2, SOF_2, SO_2F_2 based on DFT study. *Phys. E* **2020**, *122*, 114224. [CrossRef]
36. Wang, J.X.; Zhou, Q.; Lu, Z.R.; Wei, Z.J.; Zeng, W. Adsorption of H_2O molecule on TM (Au, Ag) doped-MoS_2 monolayer: A firstprinciples study. *Phys. E* **2019**, *113*, 72–78. [CrossRef]
37. Zhang, Y.J.; Zeng, W.; Li, Y.Q. Hydrothermal synthesis and controlled growth of hierarchical 3D flowerlike MoS_2 nanospheres assisted with CTAB and their NO_2 gas sensing. *Appl. Surf. Sci.* **2018**, *455*, 276–282. [CrossRef]
38. Cui, H.; Jia, P.F. Doping effect of small Rhn (n = 1–4) clusters on the geometric and electronic behaviors of MoS_2 monolayer: A firstprinciples study. *Appl. Surf. Sci.* **2020**, *526*, 146659. [CrossRef]
39. Zhou, Q.; Hong, C.X.; Yao, Y.; Hussain, S.; Xu, L.N.; Zhang, Q.Y.; Gui, Y.G.; Wang, M.S. Hierarchically MoS_2 nanospheres assembled from nanosheets for superior CO gas-sensing properties. *Mater. Res. Bull.* **2018**, *30*, 132–139. [CrossRef]

40. Zhang, Y.J.; Zeng, W.; Li, Y.Q. The hydrothermal synthesis of 3D hierarchical porous MoS_2 microspheres assembled by nanosheets with excellent gas sensing properties. *J. Alloys Compd.* **2018**, *307*, 355–362. [CrossRef]
41. Wei, Z.J.; Zhou, Q.; Zeng, W. Hierarchical WO_3-NiO microflower for high sensitivity detection of SF_6 decomposition byproduct H_2S. *Nanotechnology.* **2020**, *31*, 215701. [CrossRef] [PubMed]
42. Gui, Y.G.; Liu, D.K.; Li, X.D.; Tang, C.; Zhou, Q. DFT-based study on H_2S and SOF_2 adsorption on Si-MoS_2 monolayer. *Results Phys.* **2019**, *13*, 102225. [CrossRef]
43. Zhou, Q.; Chen, W.G.; Li, J.; Peng, S.D.; Lu, Z.R.; Yang, Z.; Xu, L.N. Highly sensitive hydrogen sulfide sensor based on titanium dioxide nanomaterials. *J. Nanoelectron. Optoelectron.* **2018**, *2417*, 1784–1788. [CrossRef]
44. Zhao, B.; Li, C.Y.; Liu, L.L.; Zhou, B.; Zhang, Q.K.; Chen, Z.Q.; Tang, Z. Adsorption of gas molecules on Cu impurities embedded monolayer MoS2: A first-principles study. *Appl. Surf. Sci.* **2016**, *158*, 280–287. [CrossRef]
45. Wang, J.X.; Zhou, Q.; Xu, L.N.; Gao, X.; Zeng, W. Gas sensing mechanism of dissolved gases in transformer oil on Ag-MoS2 monolayer. *Phys. E* **2019**, *118*, 113947. [CrossRef]
46. Sahoo, M.P.K.; Wang, J.; Zhang, Y.J.; Shimada, T.; Kitamura, T. Modulation of gas adsorption and magnetic properties of monolayer-MoS_2 by antisite defect and strain. *J. Phys. Chem. C.* **2016**, *120*, 14113–14121. [CrossRef]
47. Qian, H.; Lu, W.H.; Wei, X.X.; Chen, W.; Deng, J. H_2S and SO_2 adsorption on Pt-MoS_2 adsorbent for partial discharge elimination: A DFT study. *Results Phys.* **2019**, *12*, 107–112. [CrossRef]
48. Park, J.; Mun, J.H.; Shin, J.S.; Kang, S.W. Highly sensitive two-dimensional MoS_2 gas sensor decorated with Pt nanoparticles. *R. Soc. Open Sci.* **2018**, *12*, 181462. [CrossRef]